

Ground-based mesospheric temperatures at mid-latitude derived from O₂ and OH airglow SATI data: Comparison with SABER measurements

M.J. López-González^{a,*}, M. García-Comas^a, E. Rodríguez^a, M. López-Puertas^a, M.G. Shepherd^b, G.G. Shepherd^b, S. Sargoytchev^b, V.M. Aushev^c, S.M. Smith^d, M.G. Mlynczak^e, J.M. Russell^f, S. Brown^b, Y.-M. Cho^b, R.H. Wiens^g

^a*Instituto de Astrofísica de Andalucía, CSIC, P.O. Box 3004, E-18080 Granada, Spain*

^b*CRESS, York University, 4700 Keele St., North York, Ont., Canada M3J 1P3*

^c*Institute of Ionosphere, Ministry of Education and Science, Almaty 050020, Kazakhstan*

^d*Centre for Space Physics, Boston University, Boston, MA 02215, USA*

^e*NASA Langley Research Center, Hampton, VA, USA*

^f*Hampton University, Hampton, VA, USA*

^g*Toronto, Ont., Canada*

Received 30 January 2007; received in revised form 28 May 2007; accepted 14 July 2007

Available online 25 July 2007

Abstract

Rotational temperatures obtained from the O₂ Atmospheric (0–1) nightglow band and from the OH (6–2) band, with a Spectral Airglow Temperature Imager (SATI) instrument at Sierra Nevada Observatory (37.06°N, 3.38°W) are presented. A revision of the temperatures obtained from the Q branch of the (6–2) Meinel band has been undertaken. First, new experimental Einstein coefficients for these lines have been introduced and the temperatures derived from the Q lines (1, 2 and 3) of the (6–2) OH Meinel band have been compared to those deduced from the P lines (2 and 4) of the same band of spectra taken by a spectrograph at Boston University. The new set of SATI data has been used to analyse the seasonal behaviour of the mesospheric and lower thermospheric temperatures. Atmospheric temperatures deduced from SATI and from satellite observations with the Sounding of the Atmosphere using Broadband Emission Radiometry (SABER) instrument on board the TIMED satellite, have also been compared. SABER temperatures at 95 km are slightly warmer (about 2.5 K) than SATI temperatures while at 87 km they are slightly colder (about 5.7 K). Also, similar patterns of seasonal and day to day variations are found in the temperatures retrieved from both instruments at the latitude of 37°N. © 2007 Elsevier Ltd. All rights reserved.

Keywords: Mesosphere; Airglow; Temperature; Instruments

1. Introduction

The airglow was distinguished from starlight in 1901 by Newcomb. In 1931 Chapman suggested that airglow results from chemical recombination

*Corresponding author. Tel.: +34958121311; fax: +34958814530.

E-mail addresses: mariajose@iaa.es, mjlg@iaa.es (M.J. López-González).

(Chapman, 1931). Remote sensing of airglow emission has been developed over many years and ground-based measurements of airglow emissions have been largely used to obtain information on the mesosphere and lower thermosphere (80–120 km). In particular hydroxyl (OH) Meinel bands have been used to measure the temperature in the upper mesosphere since its discovery by Meinel (1950a) (see Bittner et al., 2002, and references therein). In a similar way the O₂ Atmospheric (0–1) band has also been used to sound the upper mesospheric temperature since Meinel (1950b) observed it using a spectrograph.

The Spectral Airglow Temperature Imager (SATI) instrument measures the column emission rate and vertically averaged rotational temperature of the OH (6–2) band and of the O₂ Atmospheric (0–1) band (see Wiens et al., 1997) and hence monitors the atmospheric temperature at about 87 and 95 km, where the peaks of the OH and O₂ emission layers are located, respectively (see e.g. Baker and Stair, 1988; Tarasick and Evans, 1993; McDade, 1998, and references therein). Measurements of the temperature structure of the upper atmosphere with the SATI instrument operated at Sierra Nevada, Spain, between 1998 and 2002 have been reported by López-González et al. (2004). One of the aims of this paper is to report on an improvement and validation of the method used for the retrieval of temperatures from the OH Meinel band. Thus, Pendleton and Taylor (2002) showed that the new Einstein coefficients derived by French et al. (2000) for the Q branch of the OH(6–2) band decrease with J faster than the previously available Einstein coefficients. These new experimental data have been incorporated in the present analysis.

In addition, in order to validate the SATI OH rotational temperatures, we have compared the rotational temperatures derived from the Q₁(1), Q₁(2) and Q₁(3) lines of the OH(6–2) band with those derived from the P₁(2) and P₁(4) lines of the same band. For that purpose, the nightglow spectra taken by an imaging spectrograph at Boston University (Smith et al., 2007), which measures both the Q and P lines, have been used.

Another goal of the present study is to contribute to the validation of the upper atmosphere and lower thermosphere kinetic temperatures measured by the Sounding of the Atmosphere using Broadband Emission Radiometry (SABER) instrument on the TIMED satellite (Russell et al., 1999). The SABER

instrument uses a sophisticated temperature retrieval scheme, under conditions of non-local thermodynamic equilibrium, which requires an accurate validation. A preliminary comparison of SATI temperatures with those retrieved from SABER (version 1.06) is also presented and discussed.

2. SATI instrument

SATI is a spatial and spectral imaging Fabry–Perot spectrometer in which the etalon is a narrow band interference filter and the detector is a CCD camera. It is based on the property of a narrow-band Fabry–Perot interference filter that transmits light from spectral lines of decreasing wavelength at increasing incidence angles.

The SATI optical configuration is shown in Fig. 1 (see Sargoytchev et al., 2004, for a detailed description of the instrument and its capability). A conical mirror provides an image from an annular field of view centred with an angle of 30° on the

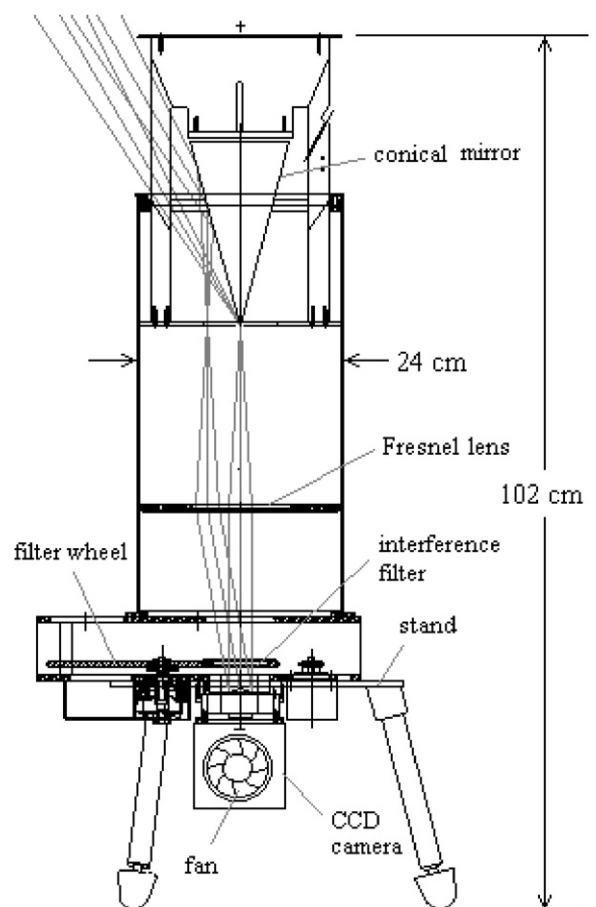


Fig. 1. SATI optical configuration.

optical axis. The Fresnel lens ensures that the entrance pupil is focused on the CCD. The Fresnel lens combined with the CCD camera lens, sets the angular width of the annulus at $7^{\circ}10'$. Thus, an annulus of average radius of 55 km and 16 km width at 95 km of altitude (or an average radius of 49 km and 14 km width at 85 km) is observed on the sky. An interference filter is interposed in front of the CCD camera to obtain the interferogram.

SATI uses two interference filters. One is centred at 867.689 nm (in the spectral region of the O₂ Atmospheric (0–1) band) and has a spectral bandwidth of 0.231 nm. The PP and PQ branches of the spectrum of the O₂ Atmospheric (0–1) band appear as pairs of lines of 0.13 nm separation, being separated from each other by 0.32 nm. These line pairs, convolved with the 0.230 nm bandpass of the interference O₂ filter, appear as single lines. Since the spectral pattern is symmetrical about the optical axis, the CCD records the lines as rings, corresponding to the $K = 3, 5, 7, 9, 11$ and 13 transitions. The second filter is centred at 836.813 nm (in the spectral region of the OH (6–2) band) and has a spectral bandwidth of 0.182 nm. The first three pairs of lines of the Q branch of the OH (6–2) Meinel band are separated from each other by about 0.7 nm with a separation of the lines in each pair from 0.1 to 0.3 nm. These line pairs, convolved with the 0.182 nm bandpass of the interference filter, produce three lines corresponding to the transitions $K = 1, 2$ and 3.

The images obtained from SATI instrument are disks where the azimuth dimension corresponds to the azimuth of the ring of the sky observed, while the radial distribution of the images contains the spectral distribution, from which the rotational temperature is inferred (see Fig. 2). The images can be analysed as a whole, obtaining an average of the rotational temperature and emission rate of the airglow band from the whole sky ring; this allows a good monitoring of the behaviour of rotational temperature and emission rate for long periods, or, by dividing the images in different sectors, obtaining information of rotational temperatures and emission rates of each sector of the sky ring.

The method of temperature and emission rate determination is described in detail by Wiens et al. (1991) for the case of O₂ atmospheric system and by López-González et al. (2004) for the case of the OH(6–2) Meinel band. The spectrum measured is compared with a set of modelled spectra for temperatures from 100 to 300 K to find the best fit

to the observed spectrum. The precision of the derived rotational temperatures is better than 2 K.

The system has been quite stable during these years of operation. The filters work at a stable temperature of 40 °C and the position of the rings from the centre of the image also seems stable. Small changes in the position of the rings from the centre have been taken into account.

A SATI instrument was installed at Sierra Nevada Observatory (37.06°N, 3.38°W), Granada, Spain, at 2900 m height on October 1998. It worked until May 2003 in a continuous and automatic mode during all no-moon night-time periods, taking exposures of 2 min alternating between the O₂ and OH filters. There has been almost a two and a half year period with no SATI data (from May 2003 to September 2005), while a new building was built for SATI housing. Since September 2005 SATI has been in operation again in a continuous and automatic mode.

3. Observations

The seasonal variation found in rotational temperatures and airglow emission rates of the O₂ Atmospheric (0–1) and of the OH Meinel (6–2) bands measured with SATI during the period from October 1998 to March 2002 has been analysed by López-González et al. (2004). A clear annual component was detected in the rotational temperatures derived from both emissions, together with a semiannual component of smaller magnitude. The OH temperatures were corrected following Pendleton and Taylor (2002), who account for the temperature-dependency of the Einstein coefficients for the Q branch. Here we have re-processed the temperature data using the experimental Einstein coefficients of the Q branch measured by French et al. (2000). The new temperatures, however, are similar to those obtained in the previous data set, with small differences in the mean temperature of only about 1 K. The Einstein coefficients derived by French et al. (2000) have also been used in the processing of the data taken since March 2002 up to date.

The SABER instrument, launched on board the TIMED satellite at the end of 2001, is a broadband infrared radiometer which measures the infrared Earth limb emission from the troposphere up to 350 km daily and near globally. The kinetic temperature profiles are retrieved from the CO₂ emission at 15 μm. This emission is affected by

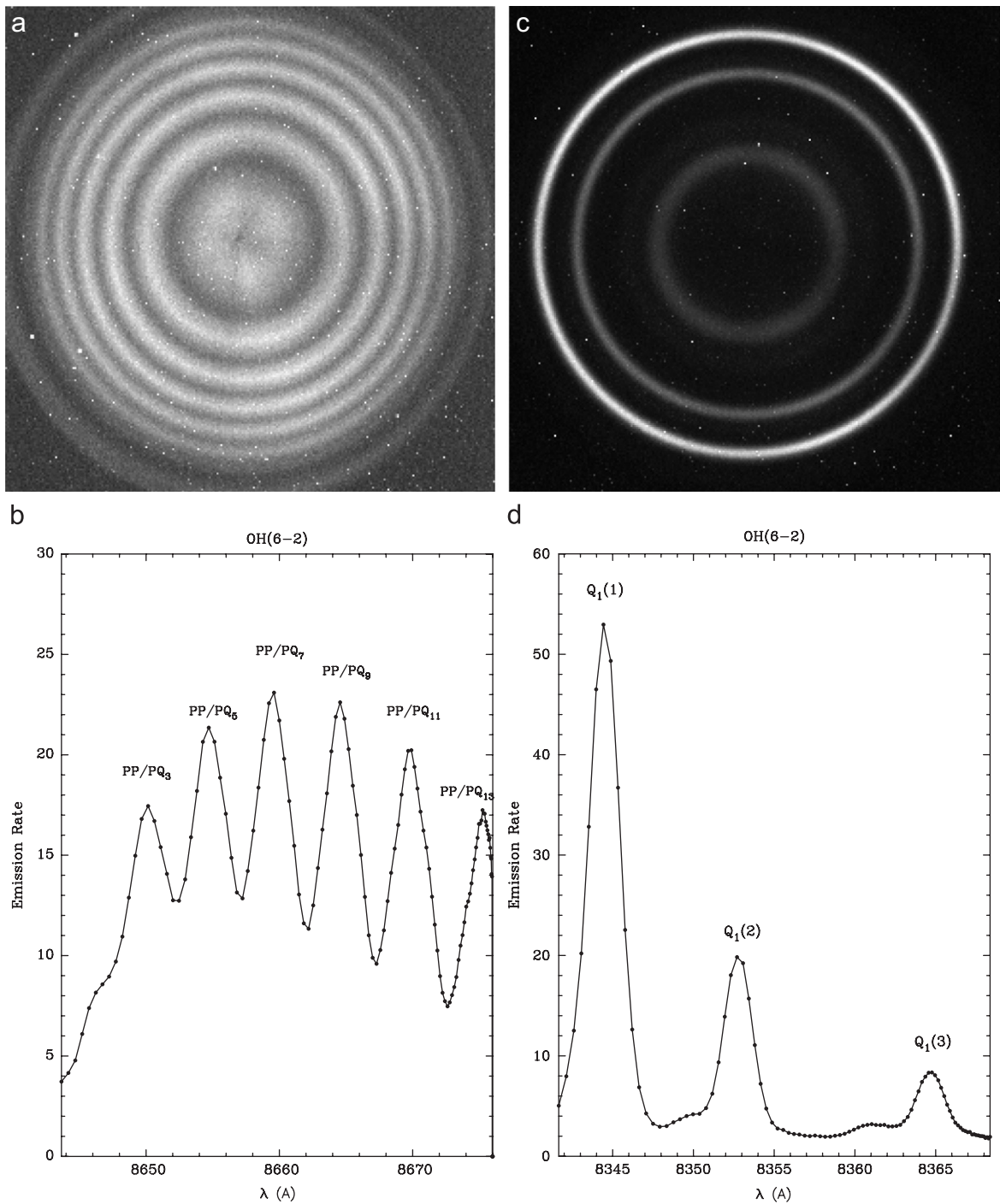


Fig. 2. Typical O₂ SATI image and the derived PP/PQ lines of the O₂(0–1) atmospheric band (left panel). Typical OH SATI image and the derived Q lines of the OH(6–2) band (right panel).

non-LTE in this low-density atmospheric region (López-Puertas et al., 1992). Hence, in order to accurately derive the kinetic temperature, it is

necessary to use a retrieval algorithm that accounts for non-LTE effects. This algorithm includes a non-LTE model which calculates the populations of the

CO₂ vibrational levels emitting at 15 and 4.3 μm including all collisional and radiative processes that affect them. The retrieval algorithm is fully discussed in Mertens et al. (2001, 2002). SABER orbits the Earth in about 90 min providing around 100 temperature profiles in that time. The non-LTE retrievals of kinetic temperature from SABER measurements (version 1.06) are compared with the temperatures inferred from SATI spectra.

4. Data analysis

4.1. Comparison of rotational temperatures inferred from the OH(6–2) Q and P branches

We have applied the method of deriving OH rotational temperature with the SATI instrument to a set of airglow spectra taken by a meridional imaging spectrograph of Boston University which operated at Millstone Hill during the 2005 summer (Smith et al., 2007), as a way to validate the rotational temperatures obtained from the Q branch of the OH(6–2) Meinel band.

Fig. 3 shows the spectral region from 833 to 860 nm, where the OH(6–2) band is located, for one spectrum measured by the Boston University spectrograph. The Q₁(1), Q₁(2) and Q₁(3) lines from the Q branch of the OH(6–2) band are easily recognized together with the lines of the P branch. Although the Q lines in these spectra have less resolution than those measured by SATI the OH rotational temperatures have been derived by applying the same method as in SATI.

The rotational temperatures derived from the ratio of the P₁(2) and P₁(4) lines, T(P) (see Smith et al., 2007) and those obtained from the Q₁(1), Q₁(2) and Q₁(3) lines following the method used in SATI and the French et al. (2000) Einstein coefficients, T(Q), are shown in Fig. 4. In general, there is a good agreement between the two temperature sets. Although the number of spectra analysed is not very large, the mean of the temperature difference obtained is very small (1 ± 8 K). These results indicate that the rotational temperatures derived from the Q₁(1) to Q₁(3) lines and from those of the P₁(2) and P₁(4) lines of the OH(6–2) band are very consistent.

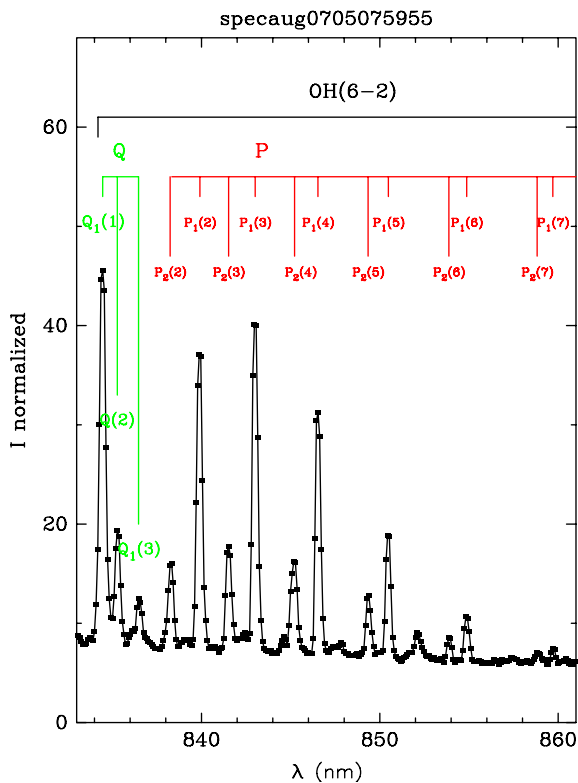


Fig. 3. One of the OH(6–2) Meinel band spectrum measured by the Boston University spectrograph on 7 August 2005.

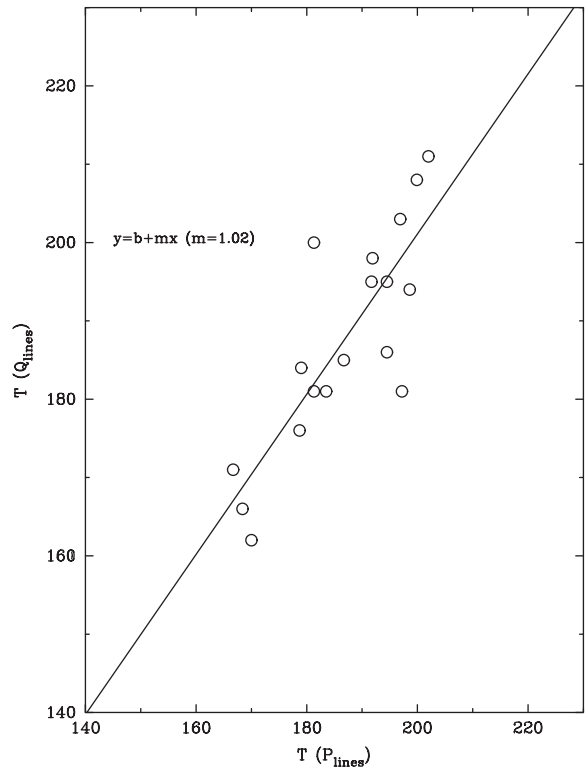


Fig. 4. OH rotational temperatures calculated from the Q branch compared with those obtained from the P branch.

4.2. Seasonal variations in temperature

Fig. 5 shows the monthly mean values of temperatures deduced at about 87 km (from OH emission) and at about 95 km (from O₂ emission) from October 1998 to July 2006. In black are the temperatures measured until March 2002 (re-processed, see Section 3). In grey are mean values obtained after March 2002 presented for the first time in this work. These monthly mean temperature values are obtained by averaging the available measurements taken during the no-moon period of each month as function of the average day of the observations.

Investigations of the mesospheric temperatures have found a clear seasonal variation. This variation is mainly semiannual at low latitudes (Takahashi et al., 1995; Taylor et al., 2005 from ground-based observations; Shepherd et al., 2004 from satellite observations) evolving to annual modulation of high amplitude at higher latitudes (Bittner et al., 2002; Shepherd et al., 2004). At middle latitudes, an annual modulation of moderate amplitude, together with a semiannual modulation of small amplitude, has been reported (Niciejewski and Killeen, 1995; She and Lowe, 1998; She et al., 2000). This semiannual component has also been detected even at high latitudes (Bittner et al., 2002; Burns et al., 2002).

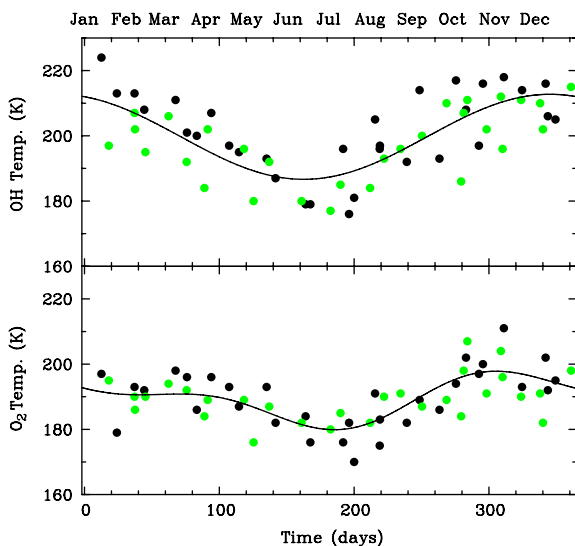


Fig. 5. SATI monthly rotational temperatures. Black solid circles: from Oct 1998 to March 2002; grey solid circles: from April 2002 to July 2006; solid lines: numerical fitting for the whole set of data.

There are important latitudinal and seasonal changes in both the altitude of the mesopause and in the mesospheric and lower thermospheric temperatures. The temperature of the mesosphere is dominated by absorption of solar radiation by O₂ and O₃, chemical heating from exothermic reactions involving odd-oxygen and odd-hydrogen species, radiative cooling associated with infrared emissions of CO₂, by turbulent heating caused by breaking gravity waves and vertical cooling associated with vertical transport of heat by dissipating waves (see e.g. States and Gardner, 2000, and references therein). The variation of the solar heating input throughout the year imposes a seasonal variation in the atmospheric parameters. The atmospheric temperature above 100 km is mainly governed by absorption of solar radiation by molecular oxygen. Then, maximum temperatures are found in summer when the solar heating is larger. In the mesosphere and lower thermosphere colder temperatures are found at high and mid-latitudes during summer. These colder temperatures are produced by the interaction of upward-travelling gravity waves with the zonal winds, which induces a meridional flow from the summer to the winter hemisphere and produces this observed annual seasonal variation in the temperature (Garcia and Solomon, 1985).

At equatorial and low-latitudes a semiannual variation is observed in mesosphere temperature. This semiannual oscillation could be produced by nonlinear advection by the meridional circulation forced by planetary waves (Garcia and Clancy, 1990).

Summer to winter temperature variations of 20–40 K have been detected at middle latitudes at 87 km (Hauchecorne et al., 1991; Senft et al., 1994; Niciejewski and Killeen, 1995; Mulligan et al., 1995; She and Lowe, 1998; Leblanc et al., 1998; She et al., 2000; Shepherd et al., 2004). Senft et al. (1994) computed harmonic fits to nightly mean lidar temperatures measured at 41°N and 40°N. They found that at 85–90 km the variation is primarily annual with maximum temperatures in winter near 205 K and minimum temperatures in summer near 180 K (i.e. an annual amplitude of about 12.5 K) while the seasonal variation at 95 km is weaker with winter temperatures near 200 K and summer temperatures near 195 K. Shepherd et al. (2004) report the annual and semiannual component fitted to daily zonal mean Wind Imaging Interferometer (WINDII) temperature values. At altitude of 9 ± 1 K for

the annual component together with an amplitude of 2.5 ± 1.4 K for the semiannual component.

The amplitudes and phases that best fit the monthly averaged SATI temperatures obtained from October 1998 to July 2006 are given in Table 1. They were obtained using the least-square fit, fitting simultaneously both the annual and the semiannual harmonics (Fig. 5, solid lines). The maximum temperatures are observed in November–January (winter solstice) while the minimum in June–July (summer solstice), consistent with the annual temperature oscillation (see, e.g. Shepherd et al., 2004). In the seasonal variation of the OH temperatures only the annual component is clearly significant. A semiannual component of small amplitude (smaller than 2 K) could be present but it is not clearly identified in this data set. However, for the O₂ temperatures, the semiannual component is larger than one-half the amplitude of the annual component. The annual amplitude that we find at 37°N is (13 ± 1 K) for the seasonal temperature variation at 87 km and a smaller annual amplitude (7 ± 1 K) at 95 km together with a semiannual amplitude of (4 ± 1 K) for the seasonal temperature variation. These results are in the range of seasonal temperature variation at mid-latitudes reported in the literature.

There is a clear difference in the seasonal variation of the O₂ and OH rotational temperatures due to the difference in the altitude region where these atmospheric emissions are located. The peak to peak amplitude is somewhat greater in OH rotational temperatures than in O₂ rotational temperatures. She et al. (2000) found that the seasonal annual variation of the atmospheric temperature with minimum values in summer at 87 km changes to maximum temperature values in summer at higher altitudes at 41°N latitude. Scheer and Reisin (1990) at 32°S and Hecht et al. (1997) at 35°S report maximum O₂ rotational temperatures in

the summer southern hemisphere and minimum in winter, opposite to the seasonal behaviour found for their OH temperatures. However, we found minima not only for the OH temperatures (87 km) but also for the O₂ temperatures (95 km) in summer at 37°N. Our observations are supported by SABER data, which also show minima at the two altitudes (see Section 4.3).

The SATI results shown here agree with the mean pattern of seasonal variation of the atmospheric temperature at mid-latitude: a moderate annual temperature variation at 87 km, together with an relative small amplitude semiannual temperature variation at 95 km.

4.3. Comparison of SATI and SABER temperatures

To compare SATI and SABER measurements, the days with SATI and SABER observations taken at geographic locations close to the SATI instrument, i.e. 37°N and 356°E, (with a coincidence criterion of $\pm 5^\circ$ in latitude and longitude and nearly identical time) have been selected.

We have selected the coincidences in SATI available data with SABER data since 2002 until July 2006. Unfortunately, no SATI measurements are available from May 2003 to October 2005, when a new building for SATI housing was built. We usually have from 1 to 4 SABER measurements for each SATI observation. These SABER temperature profiles, measured in the same satellite orbit, are averaged to obtain one mean profile at averaged latitude, longitude and temporal conditions. There are 38, 7, 6 and 28 SATI/SABER coincidences in 2002, 2003, 2005 and 2006, respectively. We are interested here in comparing the temperatures at 87 and 95 km, typical altitudes of the emission peak of the OH and O₂ atmospheric emission layers, respectively. Fig. 6 shows the temperatures obtained by SATI and SABER at those altitudes for the

Table 1
Seasonal variations in temperature

	OH		O ₂	
Mean (K)	200 ± 14		189 ± 9	
Period (years)	Amp. (K)	Pha ₀ (months)	Amp. (K)	Pha ₀ (months)
1	13 ± 1	3.7	7 ± 1	3.7
$\frac{1}{2}$			4 ± 1	4.1

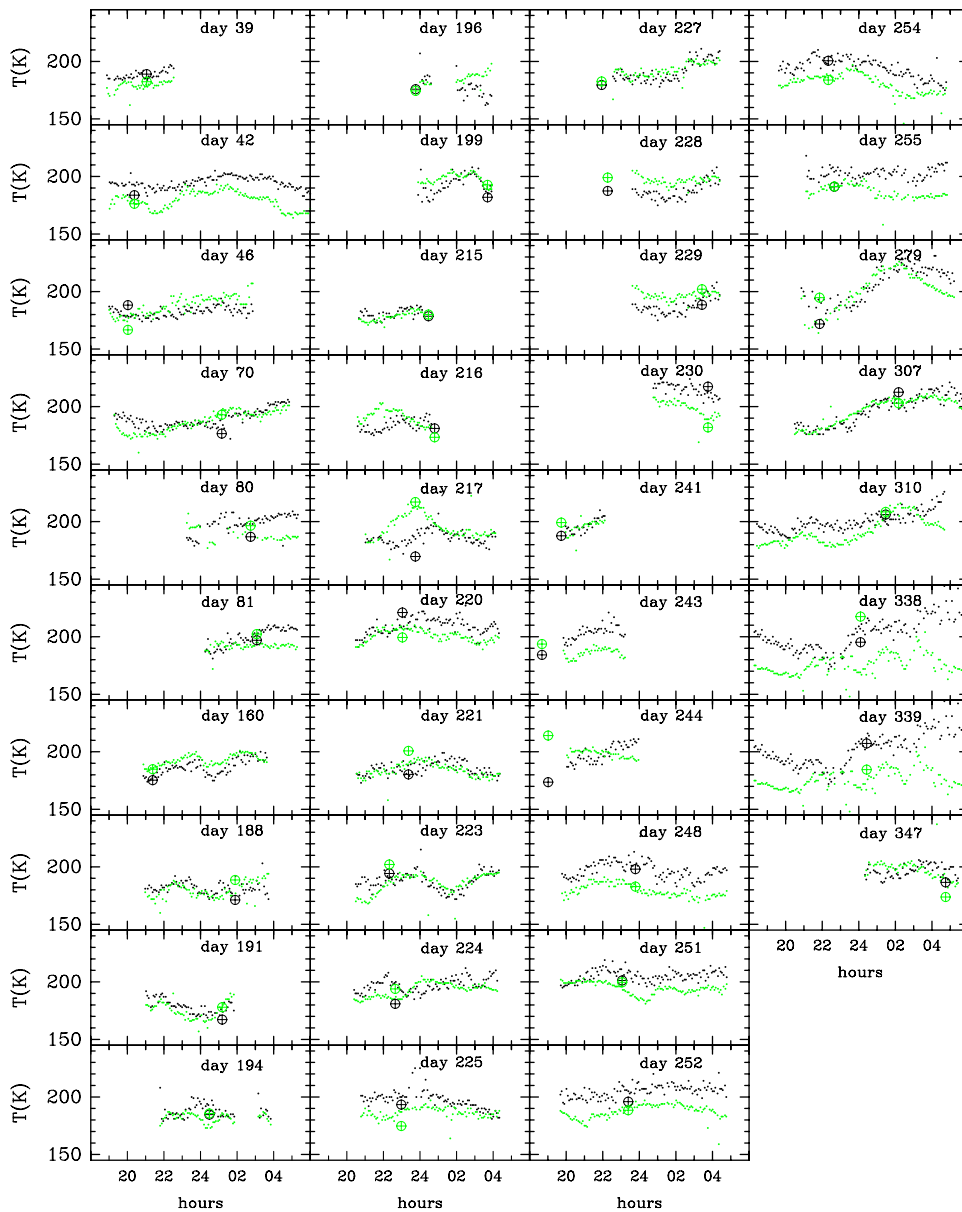


Fig. 6. SATI (dots) and SABER 1.06 (circles) night temperatures during 2002. Black: from OH; grey: from O₂; black: at 87 km; grey: at 95 km.

selected days during year 2002. The figure shows the large variability of the OH and O₂ temperatures along the night which imposes a strict temporal criterion to make the comparison meaningful.

SABER and SATI temperatures as function of the day of the year at altitudes of 87 and 95 km are shown in Figs. 7 and 8, respectively. Due to the strict coincidence criterion the number of temperature pairs is not large (79 coincidences in total). However, it is very interesting to see that, for most

of the days, SATI and SABER temperatures at 87 and 95 km seem to follow a similar variation from day to day for all years and seasons.

The temperatures of both instruments for all the coincidences of the whole period and their differences are shown in Figs. 9 and 10. Those temperatures are very similar, with a mean difference of 6.8 ± 9 K at 87 km, with SABER temperatures being colder, and a mean difference of 2.1 ± 10 K at 95 km, with SABER temperatures

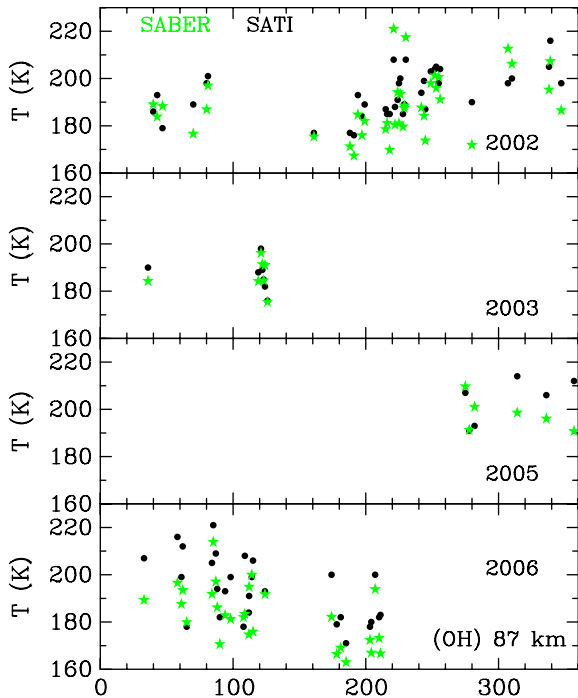


Fig. 7. Comparison of SABER and SATI temperatures at 87 km as function of the day of the year. Grey star: SABER; black solid circles: SATI.

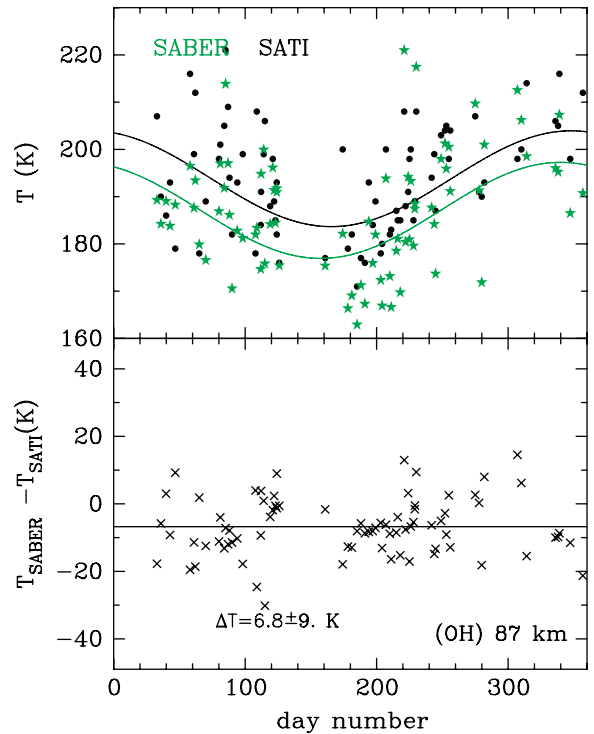


Fig. 9. Comparison of SABER and SATI temperatures at 87 km as function of the day of the year. Grey star: SABER; black solid circles: SATI; solid lines: least-squares annual fitting; bottom: temperature differences.

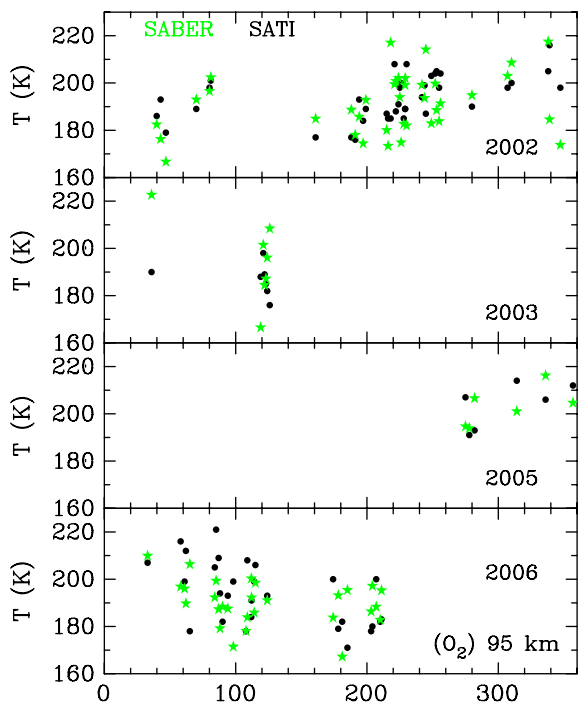


Fig. 8. Top: comparison of SABER and SATI temperatures at 95 km as function of the day of the year. Grey stars: SABER; black solid circles: SATI.

warmer than SATI. Note also that a similar seasonal variation is exhibited by the SATI and SABER temperatures at both 87 and 95 km, despite the fact that the number of coincidences is rather small to capture a seasonal variability.

We should consider also that SATI gives information on the rotational temperatures of the OH(6–2) Meinel band and of the O₂(0–1) atmospheric band, obtaining an average temperature at the altitude region where these emission layers are located. To take into account this effect we have also calculated weighted SABER temperatures at 87 and 95 km by convolving the SABER temperature profiles with typical airglow emission layers of 10 km width at half the emission maximum. In this case, the comparison between SABER and SATI is even better with a mean difference of 5.7 ± 7 K at 87 km and of 2.5 ± 7 K at 95 km for the whole period. We may emphasize the small temperature difference (smaller than 3 K) found at 95 km by both instruments.

Oberheide et al. (2006) compared three years (2003–2005) of kinetic temperatures measured by SABER with OH(3,1) rotational temperatures measured by the Ground Based Infrared P-branch

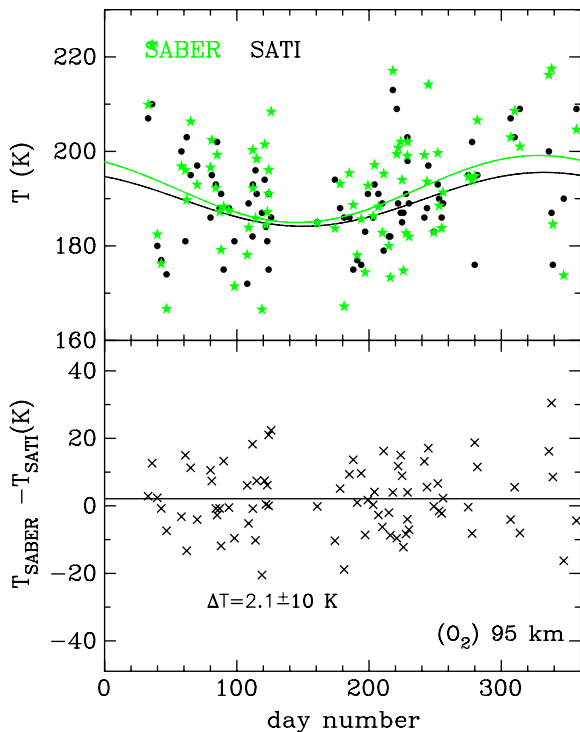


Fig. 10. Comparison of SABER and SATI temperatures at 95 km as function of the day of the year. Grey star: SABER; black solid circles: SATI; solid lines: least-squares annual fitting; bottom: temperature differences.

Spectrometer (GRIPS) placed at 51.3°N in Wuppertal, Germany and found that SABER temperatures at 87 km are colder by 7.5 ± 7.5 K than OH(3,1) rotational temperatures. Smith et al. (2007) have also compared SABER data from August and September 2005 with OH(6–2) rotational temperatures measured by the meridional spectrograph of Boston University at 42.6°N in Millstone Hill. They found an average difference between both temperatures smaller than 2 K, although the number of coincidences (22) was rather small. The differences found here for OH at a latitude 15° southward (37°N) and using a different OH band are, however, very similar to those found by Oberheide et al. (2006).

In this work, the variability of the altitude of the OH emission layer has not been taken into account in the comparison of SATI and SABER temperatures. Liu and Shepherd (2006) have shown that the altitude of the OH layer is centred near 88 km, but has a total altitude variation of 7 km. We plan to include the information of the altitude of the OH emission layer from SABER OH emission measurements and

to study the effect on the temperature difference between both instruments in a future work.

5. Conclusions

We have shown that the rotational temperatures deduced from the $Q_1(1)$, $Q_1(2)$ and $Q_1(3)$ lines of the OH(6–2) Meinel band, when using the Einstein coefficient of French et al. (2000), agree very well with those deduced from the P branch of this band.

An analysis of the seasonal variation in temperature from SATI data since 1998 to 2006 shows a clear annual variation in temperature at 87 km with minimum in summer, at maximum in winter and an amplitude of 13 K. At 95 km there is also an annual variability, with minimum in summer, but with smaller amplitude (7 K), and a 4 K amplitude semiannual component.

A preliminary comparison of SATI temperatures with temperatures from SABER shows that SABER temperatures are colder by 5.7 K at 87 km. At 95 km, the temperatures agree better, SABER temperatures being warmer by 2.5 K.

In the future we plan to use the information about the altitude of the OH emission layer, also measured by SABER, to check its effect on the temperature difference.

Acknowledgements

This research was partially supported by the Comisión Interministerial de Ciencia y Tecnología under project ESP2004-01556, the Dirección General de Investigación (DGI) under projects AYA2003-04651 and AYA2006-06375, the Junta de Andalucía, NATO under Collaborative Linkage Grants 977354 and 979480 and INTAS under the research project 03-51-6425. We very gratefully acknowledge the staff of Sierra Nevada Observatory for their help and assistance with the SATI instrument. We wish to thank the referees for their useful comments and suggestions.

References

- Baker, D.J., Stair Jr., A.T., 1988. Rocket measurements of the altitude distribution of the hydroxyl airglow. *Physica Scripta* 37, 611–622.
- Bittner, M., Offermann, D., Graef, H.H., Donner, M., Hamilton, K., 2002. An 18-year time series of OH rotational temperatures and middle atmosphere decadal variations. *Journal of Atmospheric and Solar-Terrestrial Physics* 64, 1147–1166.

- Burns, G.B., French, W.J.R., Greet, P.A., Phillips, F.A., Williams, P.F.B., Finlayson, K., Klich, G., 2002. Seasonal variations and inter-year trends in 7 years of hydroxyl airglow rotational temperatures at Davis station (69S,78E), Antarctica. *Journal of Atmospheric and Solar-Terrestrial Physics* 64, 1167–1174.
- Chapman, S., 1931. Some phenomena in the upper atmosphere. *Proceedings of the Royal Society of London* 132, 353.
- French, W.J.R., Burns, G.B., Finlayson, K., Greet, P.A., Lowe, R.P., Williams, P.F.B., 2000. Hydroxyl (6–2) airglow emission intensity ratios for rotational temperature determination. *Annales Geophysicae* 18, 1293–1303.
- Hauchecorne, A., Chanin, M.-L., Keckhut, P., 1991. Climatology and trends of the middle atmospheric temperature (33–87 km) as seen by Rayleigh lidar over the south of France. *Journal of Geophysical Research* 96, 15297–15309.
- García, R.R., Clancy, R.T., 1990. Seasonal variation in equatorial mesospheric temperatures observed by SME. *Journal of the Atmospheric Sciences* 47, 1666–1673.
- García, R.R., Solomon, S., 1985. The effect of breaking gravity waves on the dynamics and chemical composition of the mesosphere and lower thermosphere. *Journal of Geophysical Research* 90, 3850–3868.
- Hecht, J.H., Walterscheid, R.L., Woithe, J., Campbell, L., Vicent, R.A., Reid, I.M., 1997. Trends of airglow imager observations near Adelaide, Australia. *Geophysical Research Letters* 24, 587–590.
- Leblanc, T., McDermid, I.S., Keckhut, P., Hauchecorne, A., She, C.Y., Krueger, D.A., 1998. Temperature climatology of the middle atmosphere from long-term lidar measurements at middle and low latitudes. *Journal of Geophysical Research* 103, 17191–17204.
- Liu, G., Shepherd, G.G., 2006. An empirical model for the altitude of the OH nightglow emission. *Geophysical Research Letters* 33, L09805.
- López-González, M.J., Rodríguez, E., Wiens, R.H., Shepherd, G.G., Sargoytchev, S., Brown, S., Shepherd, M.G., Aushev, V.M., López-Moreno, J.J., Rodrigo, R., Cho, Y.-M., 2004. Seasonal variations of O₂ atmospheric and OH(6–2) airglow and temperature at mid-latitudes from SATI observations. *Annales Geophysicae* 22, 819–828.
- López-Puertas, M., López-Valverde, M.A., Rinsland, C.P., Gunson, M.R., 1992. Analysis of upper atmosphere CO₂ (ν₂) vibrational temperatures retrieved from ATMOS/Space-lab 3 observations. *Journal of Geophysical Research* 97, 20469–20478.
- McDade, I.C., 1998. The photochemistry of the MLT oxygen airglow emissions and the expected influences of tidal perturbations. *Advances in Space Research* 21, 787–794.
- Meinel, A.B., 1950a. OH emission bands in the spectrum of the night sky. I. *Astrophysical Journal* 111, 555–564.
- Meinel, A.B., 1950b. O₂ emission bands in the infrared spectrum of the night sky. *Astrophysical Journal* 112, 464–468.
- Mertens, C.J., Mlynczak, M.G., Lopez-Puertas, M., Wintersteiner, P.P., Picard, R.H., Winick, J.R., Gordley, L.L., Russell III, J.M., 2001. Retrieval of mesospheric and lower thermospheric kinetic temperature from measurements of CO₂ 15 m Earth limb emission under non-LTE conditions. *Geophysical Research Letters* 28, 1391–1394.
- Mertens, C.J., Mlynczak, M.G., Lopez-Puertas, M., Wintersteiner, P.P., Picard, R.H., Winick, J.R., Gordley, L.L., Russell III, J.M., 2002. Retrieval of the kinetic temperature and carbon dioxide abundance from non-local thermodynamic equilibrium limb emission measurements made by the SABER experiment on the TIMED satellite. In: *Proceedings of SPIE, Remote sensing of Clouds and the Atmosphere VII*, Agia, Greece, vol. 48882, 2002, pp. 162–171.
- Mulligan, F.J., Horgan, D.F., Galligan, J.G., Griffin, E.M., 1995. Mesopause temperatures and integrated band brightness calculated from airglow OH emissions recorded at Maynooth (53.2°N, 6.4°W) during 1993. *Journal of Atmospheric and Solar-Terrestrial Physics* 57, 1623–1637.
- Niciejewski, R.J., Killeen, T.L., 1995. Annual and semi-annual temperature oscillations in the upper mesosphere. *Geophysical Research Letters* 22, 3243–3246.
- Oberheide, J., Offermann, D., Russell III, J.M., Mlynczak, M.G., 2006. Intercomparison of kinetic temperature from 15 μm CO₂ limb emissions and OH*(3,1) rotational temperature in nearly coincident air masses: SABER, GRIPS. *Geophysical Research Letters* 33, L14811.
- Pendleton Jr., W.R., Taylor, M.J., 2002. The impact of L-uncoupling on Einstein coefficients for the OH Meinel (6,2) band: implications for Q-branch rotational temperatures. *Journal of Atmospheric and Solar-Terrestrial Physics* 64, 971–983.
- Russell, J.M., Mlynczak, M.G., Gordley, L.L., Tansock, J.J., Esplin, R.W., 1999. Overview of the SABER experiment and preliminary calibration results. In: Larar, A.M. (Ed.), *Proceedings of the SPIE Optical Spectroscopic Techniques and Instrumentation for Atmospheric and Space Research III*, vol. 3756, 1999, pp. 277–288.
- Sargoytchev, S., Brown, S., Solheim, B.H., Cho, Y.-M., Shepherd, G.G., López-González, M.J., 2004. Spectral airglow temperature imager (SATI)—a ground based instrument for temperature monitoring of the mesosphere region. *Applied Optics* 43, 5712–5721.
- Scheer, J., Reisin, E.R., 1990. Rotational temperatures for OH and O₂ airglow bands measured simultaneously from El Leoncito (31°48'S). *Journal of Atmospheric and Solar-Terrestrial Physics* 52, 47–57.
- Senft, D.C., Papen, G.C., Gardner, C.S., Yu, J.R., Krueger, D.A., She, C.Y., 1994. Seasonal variations of the thermal structure of the mesopause region at Urbana, IL (40°N, 88°W) and Ft. Collins, CO (41°N, 105°W). *Geophysical Research Letters* 21, 821–824.
- She, C.Y., Lowe, R.P., 1998. Seasonal temperature variations in the mesopause region at mid-latitude: comparison of lidar and hydroxyl rotational temperatures using WINDII/UARS OH height profiles. *Journal of Atmospheric Solar-Terrestrial Physics* 60, 1573–1583.
- She, C.Y., Chen, S., Hu, Z., Sherman, J., Vance, J.D., Vasoli, V., White, M.A., Yu, J., Krueger, D.A., 2000. Eight-year climatology of nocturnal temperature and sodium density in the mesopause region (80 to 105 km) over Fort Collins, CO (41°N, 105°W). *Geophysical Research Letters* 27, 3289–3292.
- Shepherd, M.G., Evans, W.J.F., Hernandez, G., Offermann, D., Takahashi, H., 2004. Global variability of mesospheric temperature: mean temperature field. *Journal of Geophysical Research* 109 (D24), D24117.
- Smith, S.M., Baumgardner, J., Mertens, C.J., Russell, J.M., Mlynczak, M.G., Mendillo, M., 2007. Ground-based mesospheric OH temperature comparisons with simultaneous TIMED SABER temperatures over Millstone Hill. *Geophysical Research Letters*, submitted for publication.

- States, R.J., Gardner, C.S., 2000. Thermal structure of the mesopause region (80–105 km) at 40N latitude. Part I: Seasonal variation. *Journal of the Atmospheric Sciences* 57, 66–77.
- Takahashi, H., Clemesha, B.R., Batista, P.P., 1995. Predominant semi-annual oscillation of the upper mesospheric airglow intensities and temperatures in the equatorial region. *Journal of Atmospheric Solar-Terrestrial Physics* 57, 407–414.
- Tarasick, D.W., Evans, W.F.J., 1993. Review of the $O_2(a^1\Delta_g)$ and $O_2(b^1\Sigma_g^*)$ airglow emissions. *Advances in Space Research* 13, 145–148.
- Taylor, M.J., Taori, A.K., Hatch, D.R., Liu, H.L., Roble, R.G., 2005. Characterization of the semi-annual-oscillation in mesospheric temperatures at low-latitudes. *Advances in Space Research* 35, 2037–2043.
- Wiens, R.H., Zhang, S.P., Peterson, R.N., Shepherd, G.G., 1991. MORTI: a mesopause oxygen rotational temperature imager. *Planetary Space Science* 39, 1363–1375.
- Wiens, R.H., Moise, A., Brown, S., Sargoytchev, S., Peterson, R.N., Shepherd, G.G., López-González, M.J., López-Moreno, J.J., Rodrigo, R., 1997. SATI: a spectral airglow temperature imager. *Advances in Space Research* 19, 677–680.